

Localization of Three-Dimensional Sources in Cardiac Tissue Using Optical Mapping

Gwladys Ravon^{1,2,3}, Yves Coudière^{1,2,3}, Angelo Iollo^{1,3}, Oliver Bernus², Richard D Walton²

¹ Inria Bordeaux Sud-Ouest, Bordeaux, France

² IHU Liryc, PTIB - Hôpital Xavier Arnoz, Pessac, France

³ Institut de Mathématiques de Bordeaux, Bordeaux, France

Abstract

Optical mapping allows the visualization of cardiac action potentials on cardiac tissue surfaces by fluorescence using voltage-sensitive dyes. So far, the surface measurements are directly related to surface action potentials. We aim at exploiting these measurements in order to reconstruct three-dimensional action potentials. In this preliminary work, we tried to localize fixed electrical sources in a three-dimensional slab of tissue. Therefore, we minimized the difference between the measure and a model, in a least squares sense. The model is based on the diffusion equation for the propagation of light, and simplified spherical or ellipsoidal electrical wavefronts. The inverse problem is solved by combining the gradient method and the BFGS algorithm. The method was challenged on data *in silico*, and then on experimental data. The results show improvements over previous localization methods on data *in silico*, although its use on experimental data still requires some work.

1. Introduction

Optical mapping is an important tool for the understanding of cardiac arrhythmias [1]. It provides information on the electrical behavior on the surfaces of the heart. Knowing how the depolarization front propagates inside the cardiac muscle remains challenging. So far optical mapping is used to observe optical action potential (OAP) on the surfaces or to correlate OAP upstroke morphology with the wave front orientation [2]. In [3], Khait *et al* propose a method to calculate the depth of an excitation. Their formula relies on distances from endo- and epicardium to the depolarization front. Indeed, the incident light penetrates the tissue, and the measurement contains three-dimensional information. Here we propose a method to obtain a complete three-dimensional reconstruction of the depolarization front based on the resolution of an inverse problem using optical mapping experiments. First we des-

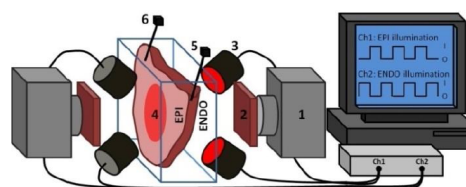


Figure 1. Schematic representation of the optical imaging setup: (1) CCD camera, (2) emission filter, (3) LED illumination, (4) tissue sample, (5) ECG electrode, (6) bipolar stimulating electrode.

cribe optical imaging setup. In paragraph 2.2 we present the forward problem used to simulate *in silico* measurements. In paragraph 2.3 the inverse problem we consider is described as well as assumptions we made on the front shape. In part 3 we present some results obtained on *in silico* and experimental data. We then conclude.

2. Methods

2.1. Optical mapping

Optical mapping can be described as follows. Fluorescent voltage-sensitive dyes that settle on the cells membrane are injected in a slab of tissue. The tissue is then put in a bath and cameras and lights are placed on both sides of the preparation (epicardium and endocardium). The lights alternatively shine the epicardium and the endocardium. The dyes in the tissue react with the incident light and the transmembrane potential (TMP) that goes through them, and emit a fluorescent light. Fluxes from this fluorescence through surfaces are captured by cameras (see set-up in Figure 1, [4]): for each illumination, fluxes are recorded on the lighted surface (reflexion) and on the opposite surface (transillumination). For each time step, optical mapping hence produces four images.

2.2. Forward problem

Cameras from the optical mapping setup capture photon fluxes through the tissue surfaces. Following the work of Khait *et al* [3] our work is based on photon diffusion theory. For each incident light, on the epicardium or the endocardium, we first solve the equation for the photon density ϕ_e of the illuminating light:

$$\begin{cases} D_e \Delta \phi_e - \mu_e \phi_e = 0 & \text{in } \Omega, \\ \phi_e + d_e \frac{\partial \phi_e}{\partial n} = 0 & \text{on } \partial\Omega \setminus \mathbb{S}, \\ \phi_e = \frac{I_e \delta_e}{D_e} & \text{on } \mathbb{S}, \end{cases} \quad (1)$$

where $\Omega \subset \mathbb{R}^3$ represents the slab of tissue, \mathbb{S} is the illuminated surface and n is the outward normal.

Afterwards, we solve the equation for the photon density ϕ of the fluorescent light:

$$\begin{cases} -D \Delta \phi + \mu \phi = \beta(V_m - V_0) \phi_e & \text{in } \Omega, \\ \phi + d \frac{\partial \phi}{\partial n} = 0 & \text{on } \partial\Omega. \end{cases} \quad (2)$$

In both equations, optical parameters $D_{(e)}$, $\mu_{(e)}$, $d_{(e)}$ stand respectively for diffusion coefficient, absorption coefficient and extrapolation distance. The attenuation length is $\delta_e = \sqrt{\frac{D_e}{\mu_e}}$. We suppose that the medium is homogeneous, so that the coefficients are constant. In equation (1), I_e represents the intensity of the illumination. In equation (2), β is a constant coefficient related to the effects of the dyes, V_m is the transmembrane potential and V_0 is the resting potential.

Finally the measured fluxes through the surfaces are given by Fick's law:

$$g = -D \frac{\partial \phi}{\partial n} \quad \text{on the epi or endocardium.} \quad (3)$$

Since the domain considered here is a rectangular slab of tissue, we could have used structured meshes. Though we choose to work with unstructured meshes: it frees ourselves from the geometry as we may use more complex tissue geometry when working on data from heart tissues. In the following experiments, we use two different meshes: a coarse one with about 20 000 points for a geometry of size $20 \times 20 \times 10$ mm, and a fine one with about 860 000 points for a geometry of size $40 \times 40 \times 20$ mm. We solve the diffusion equations with P1-Lagrange finite elements method using the solver *FreeFem++* [5].

2.3. Inverse problem

We are interested in retrieving the spatial distribution of the TMP V_m from surface optical signals on the epicardium and endocardium. Since there are less points on

the surfaces than in the three-dimensional domain Ω , the problem is under-determined. Instead of finding the complete distribution, we look for a depolarization front at each time, specifically a surface $\mathcal{S}(t)$ that splits the domain into two subdomains Ω_{rest} and Ω_{peak} . The former represents the region of tissue at rest, while the latter represents the complementary region of excited tissue.

At first, we simply choose to represent the depolarization front as an expanding sphere:

$$\mathcal{S}(t) = \{|X - X_0| - c(t - t_0) = 0\}$$

where $X_0 \in \mathbb{R}^3$ is the excitation point, $t_0 \in \mathbb{R}^+$ is the excitation time and $c \in \mathbb{R}^+$ is the constant speed. Our objective is then to identify these five parameters X_0 , t_0 and c . Therefore, for each fixed time $t > 0$, we minimize the difference $e_t(c, X_0, t_0)$ between the actual measure and the measure computed from the previous model, in a least squares sense:

$$e_t(c, X_0, t_0) = \sum_{i=1}^4 \|g_{c, X_0, t_0}^i(t) - g^{*,i}(t)\|_{L^2(\mathbb{S}_i)}^2, \quad (4)$$

where functions g are obtained by solving equations (1)-(2)-(3) and functions g^* are the data. Here i refers to one of the four images ($i \in \{1, 2, 3, 4\}$), and the surface \mathbb{S}_i is either the epicardium or the endocardium (see Table 1). This

#	illumination surface	measured surface
1	epicardium	$\mathbb{S}_1 = \text{epicardium}$
2	epicardium	$\mathbb{S}_2 = \text{endocardium}$
3	endocardium	$\mathbb{S}_3 = \text{endocardium}$
4	endocardium	$\mathbb{S}_4 = \text{epicardium}$

Table 1. References of the measures

is a natural way to define the cost function. But the value of the illumination I_e in equation (1) is not known experimentally, while the other optical parameters are. Consequently, we can only calculate the theoretical density ϕ_e , or ϕ , up to a multiplicative constant, since equations (1), (2), and (3) imply that the mapping $I_e \mapsto g^i$ is linear. So we changed the functional to the following normalized one:

$$e_t(c, X_0, t_0) = \frac{1}{2} \sum_{i=1}^4 \left\| \frac{g^i}{\|g^i\|} - \frac{g^{*,i}}{\|g^{*,i}\|} \right\|_{L^2(\mathbb{S}_i)}^2 \quad (5)$$

where the inner norms $\|\cdot\|$ are also L^2 norms on the surface \mathbb{S}_i .

A fixed-step gradient method followed by the BFGS algorithm is used to solve the inverse problem. For both functionals, we need the gradient of the cost function e_t with respect to the unknown parameters. The gradient of the first function is easily found whereas we calculate the gradient of the second one with the adjoint method.

2.4. Optical phantom

A phantom is a gel mixed with ink in order to mimic the optical properties of the cardiac tissue. In the phantom, ellipsoidal fluorescent inclusions of different sizes are integrated at various depths. The inclusions mimic the depolarized tissue. In the experiments these sources are fixed: the TMP distribution V_m does not vary in time. Because of this ellipsoidal shape, we changed the representation of the depolarization front to an ellipsoid, incorporating more unknown parameters.

In fact, we are now looking for a surface of the form

$$\mathcal{S} = \left\{ \frac{(x - x_0)^2}{r_x^2} + \frac{(y - y_0)^2}{r_y^2} + \frac{(z - z_0)^2}{r_z^2} - 1 = 0 \right\},$$

that delimits the regions Ω_{peak} and Ω_{rest} , and our theoretical TMP distribution is

$$V_m(x) = \begin{cases} 1 & \text{for } x \in \Omega_{peak}, \\ 0 & \text{for } x \in \Omega_{rest}. \end{cases}$$

3. Results

3.1. *In silico* data

We first test our method on data *in silico*: for a spherical expanding inclusion using the first proposed functional, and for an elliptic static one using the second functional.

3.1.1. Sphere and first cost function

For X_0 , t_0 , and c fixed, we solve the equations (1), (2), and (3) so as to construct *in silico* measurements $g^*(t_1) \dots g^*(t_k)$. We then solve the inverse problem to recover the unknowns X^* and t^* . The velocity c is supposed to be known. We use only the BFGS method with the optimal step given by Wolfe's rule and the coarse mesh. The iterations are stopped when the functional is less than 10^{-10} .

We consider two cases: (a) given one instance $g^*(t_i)$ for $1 \leq i \leq k$ fixed, minimize (4); (b) given $g^*(t_i)$ for all $i = 1 \dots k$, minimize the sum of (4) for $i = 1 \dots k$.

In Figure 2, we present results for the localization of the source in case (a) in function of time ($i = 1 \dots k$). Results are presented for inclusions at four different locations, excitation time $t_0 = 0$ and velocity $c = 0.5$ mm/ms. The green lines represent results obtained by our method, while the red ones are obtained using the formula from Khait's paper [3]. The vertical dashed lines mark the breakthrough of the wave on the observed surface. The last example was carried out on a general rounded geometry, to illustrate the possibility of the method.

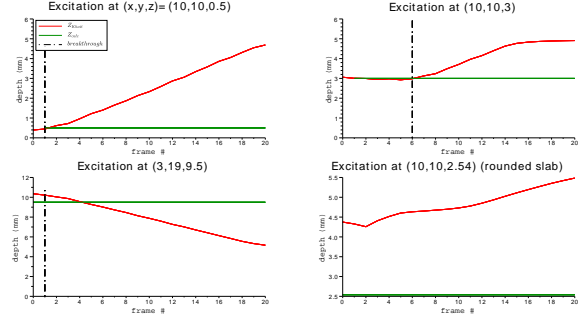


Figure 2. Comparison with Khait's approach.

In both cases (a) and (b) we retrieve the values of the unknowns with an accuracy up to machine precision. For case (a) the method converges even after the breakthrough (Fig. 2) and in case (b) we can also retrieve the value of the velocity c .

3.1.2. Ellipsoid and second cost function

Here, we fix a location $X_0 = (x_0, y_0, z_0)$ and the three radius $R_0 = (r_x, r_y, r_z)$ of the excited ellipsoid, use the forward problem to simulate the observation and the inverse problem to recover the data, based on the second, normalized, cost function (5).

For the tests, we started with a fixed-step gradient method and continued with the BFGS method after the gradient method has reached its best accuracy. We used the fine mesh.

Figure 3 shows results for an inclusion located at $X_0 = (3, 19, 14)$, and with radius $R_0 = (2, 2, 5)$. The numerical solution of the inverse problem is $X^* = (3.02, 19, 13.94)$ and $R^* = (1.64, 1.52, 4.97)$. Although less accurate than in the previous case, the difference is acceptable for application and not visible on the pictures.

In this particular case, the error reaches 25% for radius r_x and r_y because the inclusion was close to the edge. Indeed on both surfaces the signal is cut and not entirely visible.

For inclusions far enough from the edges, we retrieved all our unknowns up to machine precision as previously.

3.2. Optical phantoms

Afterwards, the method was tested on experimental optical phantoms to explore its practical possibilities and robustness. The experimental data were first smoothed by fitting them to a Gaussian. The inverse problem for the normalized cost function was solved like in section 3.1.2.

Figure 4 shows the results obtained for a phantom located at a depth $z_0 = 13$ mm. Although the reconstruction of the photon fluxes looks qualitatively fine (first and second rows of images), the reconstructed depth is $z^* = 16.7$

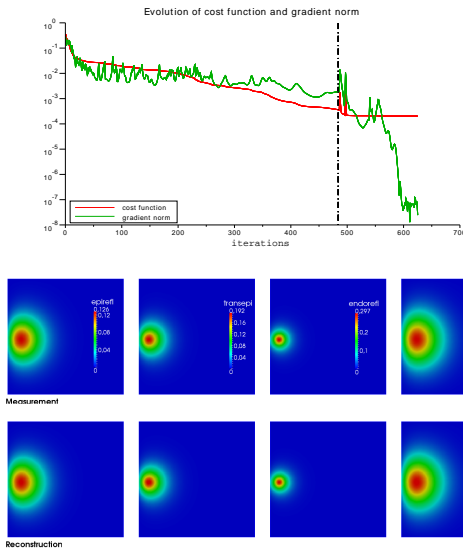


Figure 3. *In silico* experiment: cost function (and switch from gradient to BFGS at the dashed line), *in silico* observations and reconstructed observations.

mm, and the cost function remains constant after a few iterations. In order to understand this large error and evolution of the cost function, we computed the observations from the exact location of the experimental inclusion using the forward model (1) and (2) (third row of images).

These images are not coherent with the actual observation. This prompts for a reconsideration of the direct problem or the experimental setup. We have the same difficulties with seven other phantoms considered in the study.

4. Conclusion

We presented a method to localize electrical sources in three-dimensional cardiac tissues. The method combines a gradient method with the BFGS algorithm to solve an inverse problem, in order to retrieve some characteristics of the shape of the depolarization front. It allows a complete three-dimensional reconstruction of an evolving or fixed front on data *in silico*, and improve the previous results from [3]. On experimental observations, the location of the source found by solving the inverse diffusion problem does not exactly coincide with the location known experimentally. We hypothesize that there is an incoherence between the model of propagation of light (diffusion equations (1) and (2)) and the experiments. We plan to modify the direct problem, and we might improve the experimental setup (for instance by finding an experimental way to image the illumination I_e).

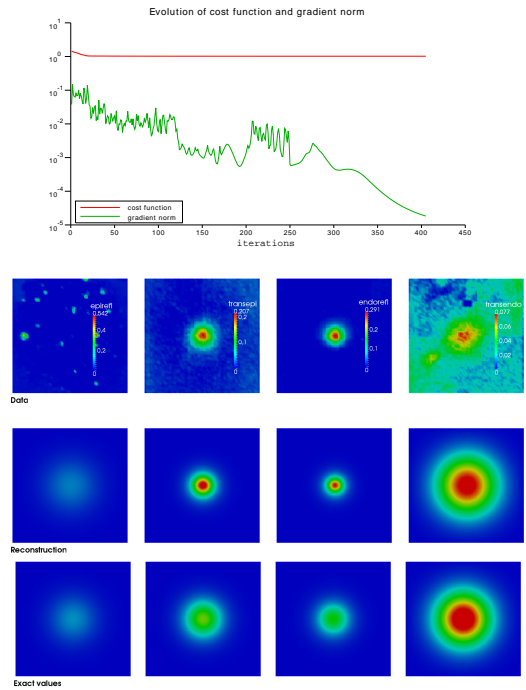


Figure 4. Results for one set of experimental data

Acknowledgments

This work is partially supported by the grant number ANR-10-IAHU-04 from the French government, and by Conseil Régional de l'Aquitaine.

References

- [1] Rosenbaum DS, Jalife J. Optical mapping of cardiac excitation and arrhythmias. Wiley-Blackwell, 2001.
- [2] Hyatt CJ, Mironov SF, Vetter F, Zemlin CW, Pertsov AM. Optical action potential upstroke morphology reveals near-surface transmural propagation direction. *Circulation Research* 2005;277–284.
- [3] Khait VD, Bernus O, Mironov SF, Pertsov AM. Method for 3-dimensional localization of intramyocardial excitation centers using optical imaging. *Journal of Biomedical Optics* 2006;11.
- [4] Walton RD, Lawrence-Xavier CD, Tachtsidis I, Bernus O. Experimental validation of alternating transillumination for imaging intramural wave propagation. *IEEE* 2011;1676–1679.
- [5] Hecht F. New development in freefem++. *J Numer Math* 2012;20(3-4):251–265. ISSN 1570-2820.

Address for correspondence:

Gwladys Ravon
gwladys.ravon@inria.fr